Attitude Control System and Star Tracker Performance of the Wide-Field Infrared Explorer Spacecraft

Russ Laher[1, 10], Joe Catanzarite[2, 10], Tim Conrow[3, 10],
Tom Correll[4, 11], Roger Chen[5, 12], Dave Everett[6, 11],
David Shupe[9, 10], Carol Lonsdale[7, 10],
Perry Hacking[8, 13], Nick Gautier[9, 14], and Ken Lebsock[5, 15]

Abstract. The Wide-Field Infrared Explorer (WIRE) spacecraft was launched into sun-synchronous orbit on March 4, 1999. An anomaly that occurred soon after successful orbital insertion rendered its science instrument useless. Nevertheless, WIRE operations have continued, utilizing the spacecraft as an engineering test bed, and for new science experiments. On-orbit data from the GSFC-developed attitude control system and Ball Aerospace CT-601 star-tracker have been analyzed to assess their performance. All applicable requirements have been met or exceeded. In particular, the results show that the pointing accuracy and stability of the spacecraft are excellent.

[1]Science Operations and Data Analysis Engineer (laher@ipac.caltech.edu)
[2]Data Analysis Engineer
[3]Lead Data Analysis Engineer
[4]Lead ACS Engineer
[5]ACS Engineer
[6]System Engineer
[7]Deputy Project Manager and Science Team Member
[8]Principal Investigator
[9]Science Team Member
[10]Infrared Processing and Analysis Center, California Institute of Technology, MS 100-22, Pasadena, CA
[11]NASA Goddard Space Flight Center, Greenbelt, MD
[12]K&D Research, Silver Spring, MD
[13]Vanguard Research, Fairfax, VA
[14]Jet Propulsion Laboratory, Pasadena, CA
[15]Orbital Sciences Corp., Beltsville, MD

Nomenclature

ACE	Attitude Control Electronics
ACS	Attitude Control System
DA	Data Analysis
FDH	Fault Detection and Handling
FOV	Field Of View
FPA	Focal Plane Array
GSFC	Goddard Space Flight Center
IPAC	Infrared Processing and Analysis Center
LEO	Low Earth Orbit
NASA	National Aeronautics and Space Administration
PID	Proportional-Integral-Differential
RMS	Root Mean Squared
SCS	Spacecraft Computer System
SMEX	Small Explorer
STP	Stellar Point
ST	Star Tracker
TDRSS	Tracking and Data Relay Satellite System
TSA	Transitional Stellar Acquisition
WIRE	Wide-Field Infrared Explorer
ZSP	Zenith Sun Point

1.0 Introduction

The Wide-Field Infrared Explorer, the fifth spacecraft developed under NASA's Small Explorer (SMEX) program, was launched on March 4, 1999 at 6:57 P.M. PST into a 540-km circular, sun-synchronous orbit by an Orbital-Sciences Pegasus XL rocket.

The spacecraft was designed to slew and stare at astronomical targets for infrared imaging, visit 10-15 different targets per orbit, and make several small pointing-offset maneuvers (usually <8 arcminutes), termed dithers, during the integration period for each target. Imaging targets at sufficient resolution places certain requirements on the spacecraft's ability to point and stay pointed at a given target. The performance of WIRE in meeting these requirements is the focus of this paper.

The spacecraft's primary mission could not be completed owing to the premature ejection of its telescope cover and consequent cryogen loss, which rendered the primary-science instrument useless. An electronics design flaw in the pyro-controller box was later found to be the cause of the anomaly. Although the rapidly venting cryogen led to a spin-up of the spacecraft, attitude control was recovered within a week.

The WIRE Attitude Control System (ACS) and Star Tracker (ST) remained fully functional beyond the nominal 4-month WIRE mission lifetime. This is also true of WIRE's other electronic systems for acquiring, processing, and downlinking image,

ACS, ST, temperature, and house-keeping telemetry data, and receiving uplinked spacecraft commands from NASA ground receiving stations. The design of the WIRE ACS system has been reviewed in detail by Fennell *et al.* (1997).[1] Characterization of the performance of such state-of-the-art ACS and ST systems in on-orbit operation has obvious importance for the design of future NASA missions.

The excellent performance of WIRE-spacecraft systems made it possible for an asteroseismology project to be put into operation, utilizing the WIRE star-tracker as a science instrument to perform long integrations on stars for detection of various oscillation modes in their intrinsic brightness (Buzasi *et al.*, 1999).[2] Subsequent ST data analysis revealed evidence of starquakes on certain target stars, proving that WIRE is still capable of good science.

Several spacecraft timelines were uploaded to the WIRE spacecraft to program its on-orbit maneuvers over a period of several months. The purpose was three-fold: 1) test and validate WIRE operations under nominal conditions (as would have been done with a functioning infrared science instrument); 2) exercise and study the performance of the ACS and ST systems; and 3) utilize the ST itself as a science instrument to collect stellar-brightness data for asteroseismology research. This report presents various WIRE ACS-and-ST system performance measures taken from the analysis of data generated in some of these operations, and compares them with the pertinent mission requirements. Since the science instrument and the star tracker would have been the only independent measurement devices of sufficient accuracy to quantify the ACS performance, some extrapolation is necessary to decide whether the pointing requirements would have been met.

First a brief overview of the WIRE mission is given, followed by descriptions of 1) the ACS and ST systems, 2) mission requirements pertinent to these systems, 3) early on-orbit mission operations, 4) the data sets analyzed, 5) the analysis methods, and 6) the analysis results. In a final section, the results are discussed and compared with the requirements.

2.0 WIRE Background Information

2.1 WIRE Mission Overview

The primary science objectives of the WIRE mission were to study the evolution of starburst galaxies and to search for ultra-luminous protogalaxies[3]. To accomplish these objectives, deep infrared images covering up to 1000 square degrees (about 3% of the sky) were to be obtained at wavelengths of 25 and 12 microns. The science instrument designed to record these data consisted of a 30-cm telescope imaging a half-degree field of view onto two infrared detector arrays, cooled by a solid-hydrogen cryostat to 12 K for the optics and 7 K for the detectors. Cumulative exposure times of several hours were specified to reach the desired sensitivity.

The science requirements coupled with the constraints of a Small Explorer mission led to several features of note for this report. The need to stare at fixed celestial targets required a three-axis-stabilized spacecraft with reasonably good pointing (see requirements section below). Keeping the telescope and the rest of the cryostat interior pointed away from the Earth and Sun in low-Earth orbit led to a Sun-synchronous polar orbit, and orbit "segments" of about 10 minutes in duration for staring at each celestial target located approximately perpendicular to the Sun-Earth line. Figure 1 shows a schematic of the on-orbit configuration of the spacecraft. Substantial design details and photographs are available at http://sunland.gsfc.nasa.gov/smex/wire/mission.

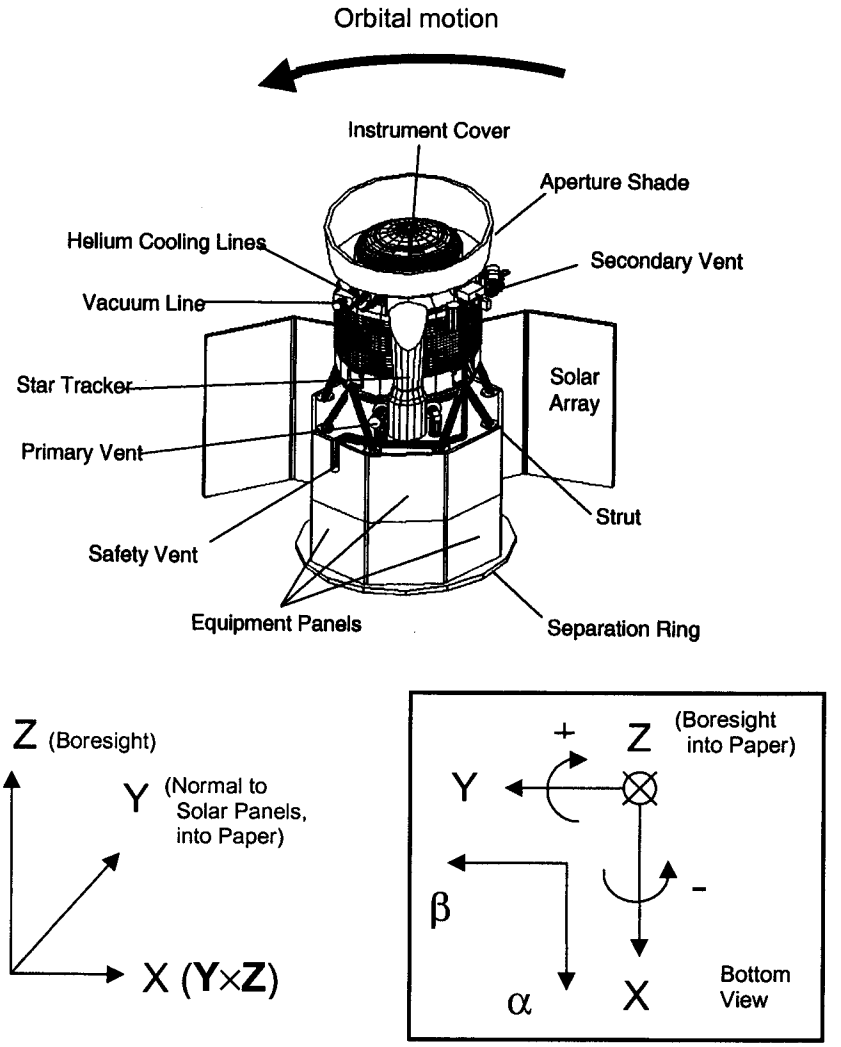

Figure 1. WIRE spacecraft on-orbit configuration.

The WIRE mission is managed by Goddard Space Flight Center (GSFC), which also built the spacecraft bus and its subsystems (power, command and data handling, attitude control, etc.). The WIRE instrument was managed by the Jet Propulsion Laboratory. The instrument's prime contractor was Space Dynamics Laboratory at Utah State University, with subcontracts to Boeing for the detector arrays and Lockheed for the cryostat. Figure 2 is a photo of the assembled WIRE spacecraft at GSFC.

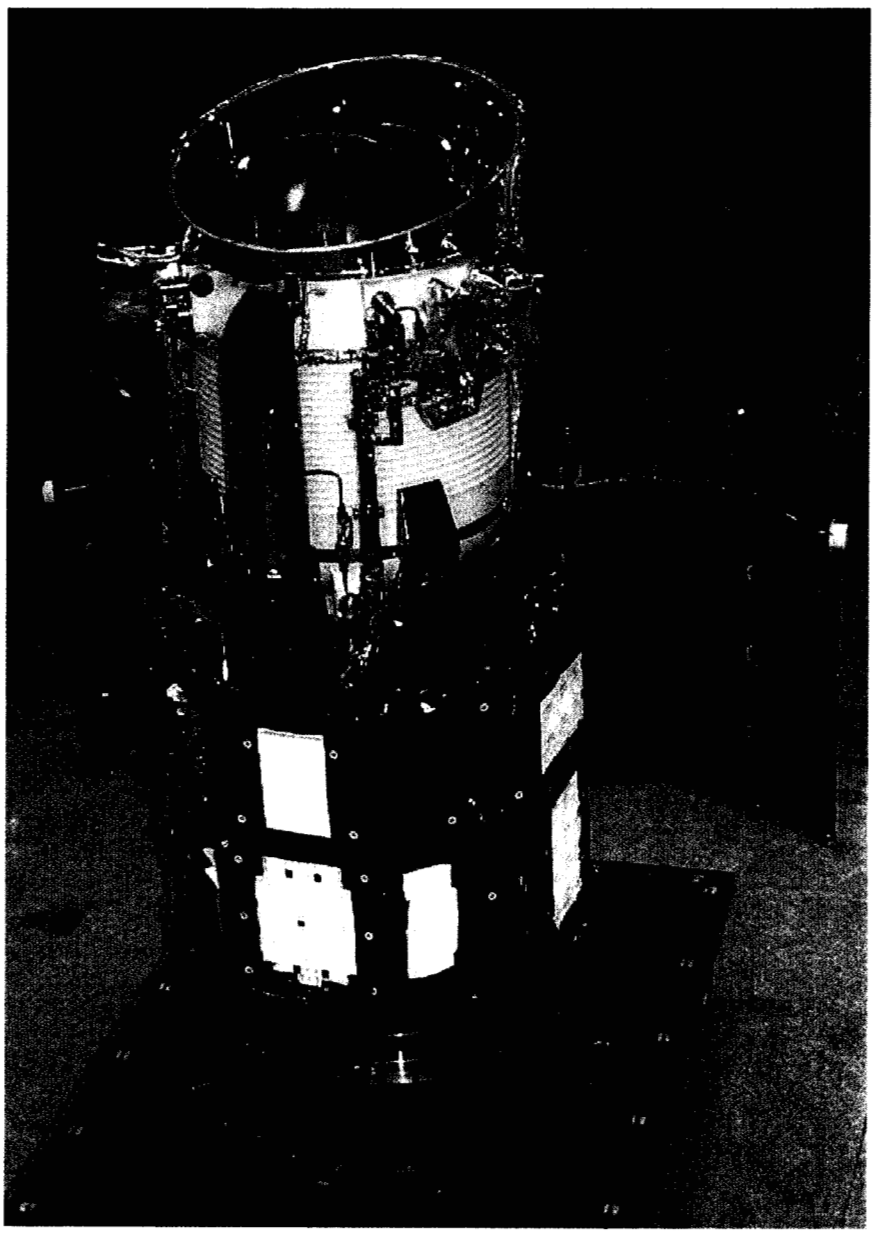

Figure 2. WIRE spacecraft at GSFC prior to launch-vehicle installation. (*Courtesy of NASA GSFC*).

To enable cumulative exposure times of several hours, the command sequencing software was designed to repeat orbit segments for each target over many consecutive orbits. This sequencing software was developed by the Infrared Processing and Analysis Center (IPAC) on the Caltech campus. Sequences are generated at IPAC and transmitted to GSFC for processing and uplinking to the WIRE spacecraft. Data are downlinked and sent to GSFC for eventual delivery to IPAC.

2.2 WIRE Attitude Control System

Only a brief review of the WIRE ACS is given here. Refer to Fennell *et al.* (1997)[1] for more details.

Besides the ST, the other attitude sensors used by the WIRE ACS are a three-axis gyro package, a three-axis fluxgate magnetometer, coarse sun sensors (6), a digital sun sensor, and a wide-angle earth sensor. The sensor signals are processed in the Spacecraft Computer System (SCS) and Attitude Control Electronics (ACE) to compute the "coarse" three-axis attitude and drive the reaction wheels (4) and magnetic torquer bars (3) for attitude control.

The WIRE ACS has six control modes, hierarchically arranged from the lowest to the highest: analog acquisition, ACE safehold, SCS safehold, Zenith Sun Point (ZSP), Transitional Stellar Acquisition (TSA), and STellar Point (STP).

Only the last two modes involve the ST. During the TSA mode, the ST attempts to lock on and track stars expected to be in its Field-Of-View (FOV), based on its coarse attitude. After the spacecraft has acquired stars, the more accurate position data from the ST becomes available to the ACS for computing a "fine" attitude. When in STP mode, the fine attitude is used for attitude determination and control; otherwise, the course attitude is used in its place.

The violation of either Sun or Earth avoidance requirements causes the Fault Detection and Handling (FDH) system to automatically switch control to a lower mode, such as from STP to ZSP.

2.3 WIRE Star Tracker

A Ball Aerospace CT-601 star tracker (ST) mounted on the anti-Sunward side of the WIRE spacecraft outside of the cryostat is used to ascertain the position of the ST's optical-axis, or boresight, based on the known positions of relatively bright and distinct stars, called "guide stars". At least two and as many as five guide stars are specified for each target. Rather than storing an onboard guide-star catalog, the guide-star positions and instrumental magnitudes are specified along with the target positions in the uploaded timelines. The ACS and ST use this information for the fine-attitude determination and control during science observations.

The actual FOV of the ST's detector is 8.2×8.2 degrees. Each square ST pixel is approximately 1.01 arcminutes on a side. Ball specifies that the ST is nominally sensitive to stars with instrument magnitudes (Mi) from 1.0 to 6.0; they confirmed this with pre-flight tests using stars down to 6.3 Mi. Our on-orbit data showed successful guide-star tracking for stars as dim as 7.5 Mi. Instrument magnitude is generally slightly smaller than visual magnitude because it includes the greater red response of the ST's Focal-Plane-Array (FPA).

The ST optical axis is mounted as parallel as possible to the telescope optical axis along the +Z body axis of the spacecraft. In practice there will be a slight misalignment between the ST and telescope optical axes, or boresights, which would have been measured using science image data and used to correct the target quaternions in the science timeline, had this been possible. For the remainder of this paper, the term boresight refers to the ST optical axis, unless otherwise noted.

2.4 ACS/ST Interactions

The ACS star-processing software processes guide-star true-position information from the timelines and feeds it to the ST for use in guide-star acquisition[4]. It also monitors ST status flags in order to ascertain which guide stars are being tracked, and it receives guide-star position data from the ST for post-processing.

The ST can simultaneously track up to five guide stars. A list of up to five guide stars is uploaded for each timeline target. The guide stars are acquired autonomously by a pattern-match method.

The first step in the star acquisition sequence is the search for a "base star." The first star in the current guide-star list, guide star 1, which is, by design, the most distinct based on its brightness and position relative to the boresight, is tested first to see if it passes muster as the "base" star. If this is an initial acquisition, the ST will be in the TSA mode, and a 2x6-degree reduced FOV is searched for the base star, knowing its position, the spacecraft's coarse attitude, and sensor geometry; an even smaller window is used for subsequent acquisitions. The tolerances for guide-star position and magnitude matching are 4 arcminutes and 1.25 magnitudes, respectively, which are stored in onboard parameter tables.

Next a search for a "second" star commences. Using the position of the base star as a reference, the relative position of the second star in the current guide-star list, guide star 2, is checked in an 8x8-arcminute directed search window. If the second star is not found, then guide stars farther down in the list are sought after until one is found.

If the list is exhausted without finding a second star, then the base star is abandoned, and guide star 2 becomes the base star candidate. The cycle through the list of guide stars is then repeated to find a second star. Once a base star and a second star are found, the

verification is complete, and directed searches for the remaining guide stars in the list are done.

As a final step, the "Good Star Condition" must be met, in which the pairwise sum of the squares of the distances among all star being tracked must be greater than 4 degrees squared. The Good Star Condition assures that the guide stars are sufficiently separated for accurate three-axis determination. Note that satisfying the Good Star Condition does not necessarily require finding all the guide stars.

The guide-star positions measured by the ST are processed sequentially by a modified Kalman filter in order to generate a noise-filtered fine-attitude solution for the ST's optical axis. This result is fed into a proportional-integral-differential (PID) controller, which computes the attitude adjustments needed for either staring at a target, or dithering from one position to another within several arcminutes of the target.

2.5 Pertinent WIRE Mission Requirements

The WIRE mission requirements that affected the star-tracker selection and ACS design included those for pointing accuracy and stability; Sun, Earth, and Moon avoidance; safeholding; and maximizing mission lifetime.[5] As with all SMEX missions, other significant factors are cost, power, mass, and delivery schedule.

The absolute accuracy requirement for WIRE was to point the telescope within 1 arcminute (1-σ) of a specified position (given in J2000 coordinates); the goal was 2 arcseconds. The roll accuracy requirement was to point within 9.5 arcminutes (1-σ) of the specified roll angle about the telescope boresight (nominal body Z-axis). It was expected that much of these errors would be due to thermally-induced random misalignment between the telescope and the star tracker.

A relative accuracy of 3.87 arcseconds (1-σ) for pointing and 18 arcminutes (1-σ) for roll was required between successive dithers.

The Root-Mean-Squared (RMS) radial dispersion about the mean position of all pixels was required to be less than 6 arcseconds during a 64-second exposure. The error was to remain less than 8.5 arcseconds more than 86% of the time (Gaussian case for 6-arcsecond radial dispersion).

The science-instrument Sun avoidance requirement was to maintain the angle between the telescope boresight and the Sun-limb greater than 75 degrees at all times during the mission to protect the science instrument from damage and to conserve cryogen. It was also required that during normal operations the Sun be kept within 3 degrees of azimuth about the boresight from the highest point of the aperture shade. These two avoidance constraints were used as requirements for the FDH system. In addition to the Sun avoidance constraints, it was required that the solar arrays be maintained within 30 degrees of the Sun's center for sufficient power input.

The Earth avoidance requirement was to keep the science telescope axis within 30 degrees of zenith. This requirement was to limit the thermal input to the cryostat. More stringent operational requirements were placed on target selection to prevent direct illumination of the aperture shade by the Earth limb. This particular requirement became irrelevant with the loss of the original science mission.

Similarly an operational requirement for moon avoidance requirement for the primary-science mission of 40 degrees from the Moon's center was set because for angles <40 degrees, the science-instrument's stray-light requirement would not be met. For all other observation types (outside of the primary-science mission), the Moon avoidance requirement was 8 degrees.

The slew-rate and settling requirements mandated the capability of slewing 72 degrees and settling within the pointing accuracy and stability requirements in less than 3 minutes.

At all times, pointing the spacecraft optical axis near zenith, and the solar arrays toward the Sun, was considered to be a safe attitude. This is how the spacecraft is to be continuously pointed while in ZSP mode, during which time the ACS ignores targets specified in the timelines. This ACS control mode was used to "safe" the spacecraft whenever a timeline target was not acquired.

Mission lifetime is also severely affected by the attitude of the spacecraft. A mission lifetime of at least 4 months was expected, based on the available cryogen. Mission modeling showed that pointing the telescope slightly out of the orbit plane in the sunward direction minimized the heat load on the cryostat due to Earthshine. Although not strictly a requirement, this consideration was taken into account in planning the observations, and in the design of the ZSP mode.

3.0 Initial On-Orbit Operations

The initial schedule of WIRE-spacecraft ground passes allowed contact for an average of 9 minutes out of every 48 minutes (or out of every 96 minutes when some ground stations were unavailable). Recorded data did not become available until several hours into the mission. Thus, as is normal for Low-Earth-Orbiting (LEO) spacecraft that do not use the TDRSS communications system, initial operations were heavily based upon a succession of 'snapshot' views of the satellite's behavior acquired during the ground passes.

The WIRE instrument was designed to use a two-stage solid-hydrogen cryostat to keep its detector cooled to below 13 K throughout the primary mission operations (nominally, the first four months). The cryostat was equipped to vent sublimated (or vaporized) gas from each of their stages. The WIRE cryostat's secondary stage, with the larger expected gas flow, was vented through a 'thrust nullifier' – a pairing of vents designed to minimize the thrust and torque produced by releasing equal amounts of hydrogen gas in opposite

directions. The WIRE cryostat's primary stage simply used an open pipe as a vent. Safety concerns forced the designers to close these cryogen vents during the launch; however, the vents needed to be quickly opened after orbit insertion to avoid over-pressure conditions within the cryostat. Ground commands were transmitted early in the first pass to open the secondary vent; and, the primary vent was opened about ten minutes later by a stored command. Non-reversible actuators under the control of the instrument pyro-controller box were used to open both of these vents.

The instrument design used an ejectable radiation and thermal shield over the telescope aperture, a.k.a. the 'cover', to minimize heat and bright-source input to the instrument during launch and early orbit operations, when the instrument would not otherwise be adequately isolated from the Earth albedo or Sunlight. The nominal-operations plan was for the cover to be ejected on the third day of the mission following three-axis attitude acquisition and checkout of all spacecraft systems. Non-reversible actuators under the control of the instrument pyro-controller box were also used to release this cover.

Shortly before the commanded opening of the secondary vent, the spacecraft behavior departed from nominal. Up until that time, the stored telemetry showed that the initial tip-off rates were being damped as expected; this is the first stage of the nominal behavior of the acquisition controller used on WIRE. Following that time, the stored telemetry showed a continuous increase in spin rates without apparent explanation, despite the fact that the available telemetry still showed the correct actuator commands and responses to the sensor inputs being received.

Post-mishap investigation revealed that as soon as the instrument pyro-controller box was powered up, it commanded all actuators under its control to fire simultaneously for about 2 milliseconds, instead of according to the pre-programmed sequence. This caused ejection of the instrument thermal cover and the opening of at least one cryogen vent in the process. The primary vent may not have been opened at the time, since its thermal actuator takes longer to fire than the pyro actuators used to eject the cover. With the Earth, and later the Sun, passing through the unshielded telescope field-of-view, the heat load rapidly sublimated the cryogen. The venting cryogen produced an average disturbance over five times the torque authority of the control actuators, resulting in an uncontrollable tumble that caused all attempts to avoid further heating of the cryogen to fail. NORAD tracking data showed the cover as a separate object in orbit starting between the first and second ground passes. Additionally, all available stored spacecraft telemetry supports this explanation. Later ground testing revealed the presence of a design flaw in the pyro-controller electronics, which was determined to have been the probable cause of the mishap under on-orbit conditions.

Continuous and sometimes-desperate attempts were made to control the spacecraft tumble over the next one and a half days, but this was unsuccessful. During this time, all instrument cryogen was lost, and the instrument detector was probably damaged by exposure to direct sunlight. At the end of the venting, the spacecraft was left spinning at about 53 RPM around the major moment of inertia axis (the body-X axis), with this axis

pointing roughly inertial South. Consequently the solar arrays viewed the Sun during half of each spin cycle and the spacecraft was power positive, allowing a recovery effort to occur. Even though the primary mission was clearly a loss, the secondary mission of engineering testing, which under normal conditions was to commence after the cryogen ran out, justified the effort. A previously unanticipated asteroseismology-science mission using data from the star tracker has also been developed since that point.

During the next five days, the spacecraft rates were damped using the digital form of the acquisition controller (SCS safehold) with only the Y and Z magnetic torquer bar rate damping terms enabled. Due to the expected time lag in the elements of the control loop, it was necessary to periodically upload a new magnetometer alignment matrix that would adjust the apparent phase lag by a multiple of 90°. Finally, after the spin rate had fallen to a low-enough value on March 11, the spacecraft returned to its normal acquisition plan. It then proceeded through the ACS modes listed in Section 2.2, with transition to STP mode on March 15. Throughout this process, the spacecraft systems all performed as expected. With the exception of four previously undeveloped configuration tables, representing the magnetometer alignments, nothing had to be added to the existing onboard controller to allow it to function well beyond the conditions for which it had been designed.

Once three-axis timeline-driven fine pointing (the nominal science control mode) was initiated, and the on-orbit sensor calibrations had been performed, the spacecraft was officially turned over to the operations group for use as an engineering test-bed, and for new scientific investigations (such as the aforementioned asteroseismology program). The main results of this paper come from some of the ACS and ST data analyses that have been performed since that time, as will be described in the remainder of this paper.

4.0 On-Orbit Data Description and Analysis Methods

We statistically analyzed raw star-tracker outputs in the form of 8×8-pixel ST FPA sub-images of target stars. Further details and results of this particular analysis are given in Section 5.1. The remainder of this section pertains to many of the results presented in Section 5.2 and later.

The ACS-processed ST data that are analyzed in this paper are primarily from two different ~2-hour data sets of guide-star positions sampled at 10 Hz. The first data set was acquired on day 85 (March 26, 1999) and the second data set was acquired on day 140 (May 20, 1999). Figure 4.0-1 shows the distribution of targets pointed at by the star tracker during the acquisition of these data. For each of these targets, one or more data frames were taken during a given orbit segment. In general, the pointing was dithered a certain pseudo-random amount up to 8 arcminutes from frame to frame.

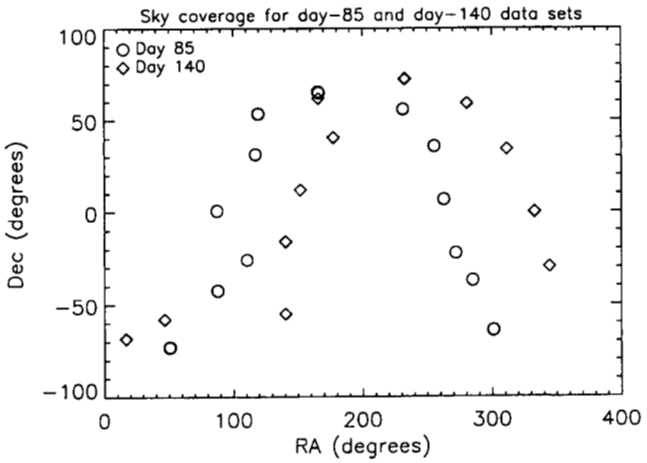

Figure 4.0-1. Sky distribution of targets associated with the data analyzed in this report. Each symbol represents one or more data frames acquired during a given orbit segment.

Within the times spanned by these two data sets, many data frames with frame times ranging from about 15 seconds to as long as ~9 minutes were taken. Figure 4.0-2 shows the number of samples per frame versus the number of frames in the two data sets. Most of the frames have frame times between 20 and 40 seconds.

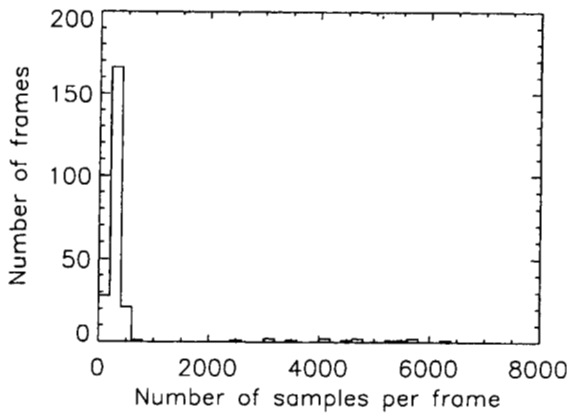

Figure 4.0-2. Histogram of number of samples per frame versus number of frames in the day-85 and day-140 data sets.

Guide-star positions, as well as a plethora of ancillary information, all sampled at 10 Hz, are available for each data frame. The measurement precision of the guide-star positions and instrument magnitudes by the star-tracker are 0.5 arcseconds and 0.0625 magnitudes, respectively.

The guide-star positions after ACS post-processing of star-tracker outputs are given in terms of two orthogonal separation angles, α and β, from the star-tracker optical axis (which is synonymous with the term boresight). Positive values of α result for positive rotations about the body Y-axis, and positive values of β result for negative rotations about the body X-axis. These angles are computed by the onboard ACS processor from the star-tracker outputs using a scale factor, A, and biases, B_1 and B_2:

$\alpha = A$ * star-tracker FPA-row output + B_1
$\beta = A$ * star-tracker FPA-column output + B_2

The ST outputs are given in ST units, or counts, and represent the digital FPA positions from the ST itself. Ball Aerospace derived the following values of A, B_1, and B_2 from least-squares fits of their ground-calibration data taken over the star-tracker's operating-temperature range of –30° C to +50° C: A=0.5 arcseconds/count, B_1=2520 arcseconds, and B_2=1080 arcseconds. Ball's assessment of their star-vector accuracy, on which the star-tracker calibration is based, is roughly 0.25 arcseconds (1 σ).[5] Note that internal to the ST, the conversion from ST FPA positions to separation angles is performed using transformations of the form arctan(x/f), where the focal length, f, is approximately 92 mm, and x is the ST FPA distance from the boresight along the dimension of the separation angle.

At each sampling time the position measurements of from 2 to 5 guide-stars are available. Figure 4.0-3 shows the nominal guide-star positions within the star-tracker FOV for all data frames in the day-85 and day-140 data sets. The distribution of positions is fairly uniform over the FOV.

Weighted least-squares fits of many sets of guide-star position measurements were made to the known values of α and β of the guide stars from the GSFC guide-star catalog constructed for the WIRE mission. A different fit was done at each sampling time. Approximately 150,000 least-squares fits were done to process all of the data from the two data sets.

Although α-β space is nonlinear, the errors between the measured and known positions are small enough that this non-linearity can be neglected (when considering only the differences between measured and known positions). The three least-squares fit parameters are an offset in α, given by C, and in β, given by D, and a rotation angle, given by E, about the star-tracker boresight position. If (α_i, β_i) are the measured guide-star positions, and (α'_i, β'_i) are the known guide-star-catalog positions for a set of N guide stars, where the index i denotes the i-th guide star in the set, then the least-squares fitting involves solving the simultaneous equations

$$\alpha'_i = \alpha_i \cos E + \beta_i \sin E + C,$$
$$\beta'_i = -\alpha_i \sin E + \beta_i \cos E + D,$$

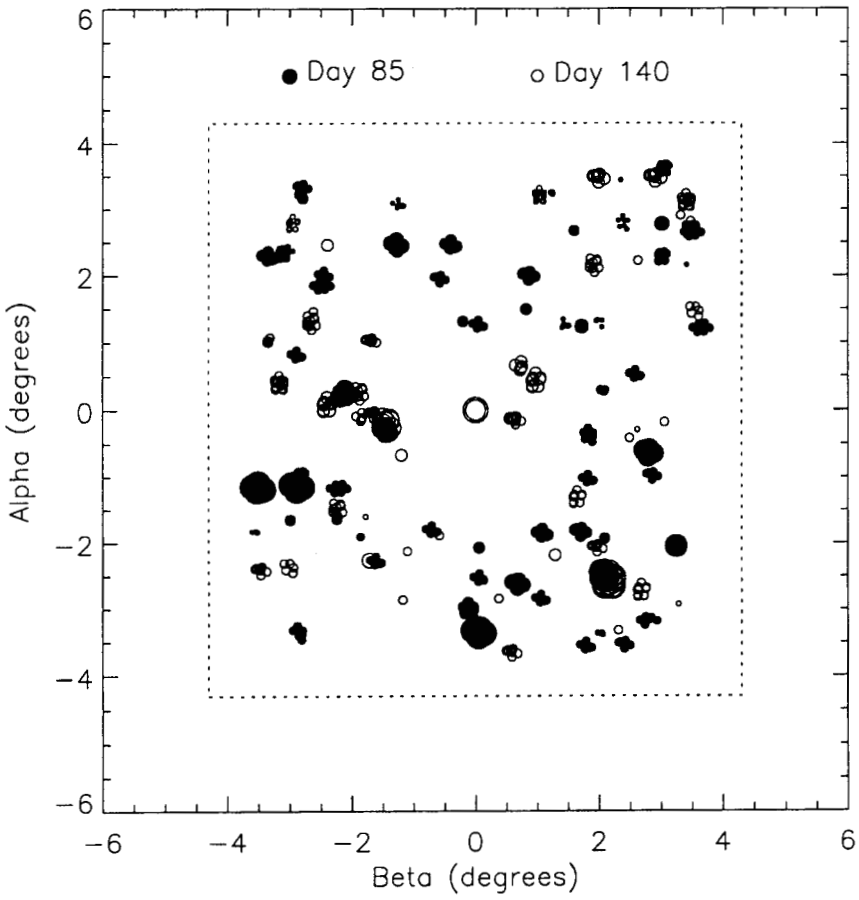

Figure 4.0-3. Nominal positions of the guide stars associated with the data frames analyzed in this report. The dotted line delimits the star-tracker FOV. The symbol size indicates the intensity of each guide star.

where i = 1,...,N. This data fitting is constructed to minimize the mean-squared error between the measured and known positions by adjusting parameters *C*, *D*, and *E*. The number of degrees of freedom of these fits, ν, are given by $2N$-3, where N is the number of guide stars for each fit. No attempt was made to reject outliers during the data-fitting process.

If the errors between measured and known positions are Gaussian-distributed, then the sum of the squared errors, normalized by the variances of the errors, will be chi-square distributed with ν degrees of freedom. For values of the variances of the input-data errors, only the variances of the measured positions, as computed over 300 or more samples local in time, were used in the fits. Possible guide-star catalog and other errors, such as distortion in the ST optics, were ignored in computing the variances of the errors in the input data.

Separate averaging of *C*, *D*, and *E* has been carried out for each data frame, in order to determine the average error between the commanded target and where the boresight actually pointed (as determined from ST data) for each frame. Sample-number-weighted averaging of the frame results has also been performed in various ways to correlate these errors with system parameters, including number of guide stars, maximum separation of guide stars, distance of brightest guide star to boresight, and magnitude of brightest guide star.

In order to assess relative errors, the dispersions in *C*, *D*, and *E* have been computed by the RMS deviations from their respective median values over a data frame. Here we have assumed that the mean is approximated by the median value. This was done to make the estimation of mean insensitive to outlier positions caused mainly by residual pointing drift, which is relatively higher in the first 100 seconds after a slew from one target to the next.

5.0 Performance Results

5.1 Raw-Data Guide-Star Position and Acquisition Analyses

This section presents some results of our analysis of raw FPA data from the WIRE ST. There are five designated 8×8-pixel regions on the ST FPA, termed slots and numbered from 0 to 4, which are centered on the guide-stars being tracked. The raw data we analyzed is from slot 0, and consists of images centered on the base guide-star. Each image is sampled at 10 Hz.

For WIRE asteroseismology observations, the timeline target and base guide-star positions are identical, and slot-0 exposures of the target star are available, provided that the target star is bright enough (see second half of this section). In this special situation, it is interesting to know whether the target star's position is repeatedly measured at the same pixel (and even sub-pixel) region on the ST's FPA, as determined from the slot-0 data. The data set analyzed was taken on 6/23/99, and includes six observations of the star Beta Crucis and five observations of the star Alpha Ursa Majoris. Both targets are relatively bright, with instrumental magnitudes of 1.7 and 1.5, respectively. Each observation consists of nearly 40 minutes (almost half a WIRE orbit) of 10-Hz-sampled slot-0 exposures, or about 20,000 exposures. The centroid for each observation of a given target was computed by flux-weighted averaging to determine its mean position. The standard deviations of these centroids were also computed. The results are given in Table 5.1-1.

Table 5.1-1. Mean centroids of slot-0 targets on the WIRE ST FPA. The standard deviation is given in parentheses.

Target star	Mean row centroid (pixel)	Mean column centroid (pixel)
Beta Crucis	258.05 (0.01)	259.72 (0.02)
Alpha Ursa Majoris	258.19 (0.01)	259.67 (0.02)

For each observation, typically 96.5% of the samples had centroids within 4 sigma of the mean centroid. Since the instantaneous FOV of a ST-FPA pixel is approximately 1.01 arcminutes, the centroid is stable to within a standard deviation of about 1 arcsecond. These results show that each target star's profile falls repeatably on essentially the same portions of the FPA array each time it is sampled.

For the asteroseismology studies being conducted with the WIRE satellite, the asteroseismology target star is also the first star in the timeline's guide-star list. It is desirable that this star also be selected by the ST as the base star, so that slot-0 exposures of this star will also be taken when sampling at the 10-Hz rate. The problem is that the ACS star-processing software does not guarantee that the first guide star in the current list will actually make it into slot 0. However, we can check the success rate by examining the ancillary data that are returned with the slot-0 exposures. The results of an analysis of data acquired on 5/11/99 and 5/12/99 are given in Table 5.1-2.

Table 5.1-2. Fraction of the time the target star populates slot 0 of the WIRE ST versus base-star magnitude.

Magnitude range	Number of base-star samples	Fraction of base-star samples populating slot-0
1-2	441	1.0
2-3	168	1.0
3-4	347	0.971
4-5	2858	0.635
5-6	2513	0.382

Based on the results of Table 5.1-2, the reliability of target star acquisition in slot 0 is excellent for guide stars down to down to magnitude 4. For target stars dimmer than this level, the reliability falls off rapidly.

In cases where the target star does not end up in slot 0, it is possible to determine from onboard processing the slot that the star was actually assigned (if any). However, this capability, which requires a software patch to be uplinked to the spacecraft, has not yet been implemented.

5.2 Guide-Star Position-Measurement Statistics

Figure 5.2-1 shows plots of α versus β for the five guide stars during the first and last frames of an observation segment. These results are fairly typical of the frames with no anomalies, which include about 90% of the frames in the two days covered by this study. Each of these frames is a little more than 30 seconds in length; since the sampling rate is 10 Hz, a little more than 300 data points are shown connected with lines, with the first point represented as a solid diamond.

In the first frame of this typical observation segment, the scatter of points is elongated along the slew direction, which is primarily in the α dimension, owing to a residual drift in the motion of the star-tracker boresight. This is typical behavior seen for frames that directly follow a slew from a previous target to the present target. The drift is present even after the settle flag has been set, albeit smaller, because the integral compensation in the control loop exponentially reduces the remaining error. (The settle flag is used to mark when the science-instrument data collection can begin.) Data for frames that are several minutes in length show that the drift decreases over time, rapidly at first and then more slowly, diminishing to insignificance after about 100 seconds. For this particular frame, the RMS deviations from the median value of α range from 1.7 to 2.7 arcseconds depending on the guide star. The corresponding RMS deviations for β range from 0.4 to 1.1 arcseconds.

In the last frame of our typical observation segment, this drift is not evident, even though the spacecraft was commanded to perform a small (<8-arcminute) dither between the next-to-the last and the last frames. For this particular frame, the RMS deviations for α and β are comparable, and range from 0.4 to 1.5 arcseconds.

The guide-star sets used for acquisition of the data shown in Figure 5.2-1 are identical between the two frames, since they are from the same observation segment. The first guide star of these frames (right and left plots at the top of the figure) has the smallest dispersions in relative RMS error in α and β. This first guide-star also happens to be the brightest of the set, which is the usual result of guide-star ordering by the WIRE scheduling software. The 0.5-arcsecond quantization in the positions can be clearly seen in the plotted positions for the first guide star. Comparing the same guide stars between the two frames shows that the measured magnitude varies by a magnitude quantization level, which is most likely a small FPA-temperature effect caused by changing solar illumination on the spacecraft as it moves along its orbit during the observations.

About 10% of the frames in the two data sets have very minor anomalies. Usually one of the guide stars associated with this small fraction of the frames has one or two measured positions that deviate 10-100 arcseconds away from its median position. More than 80% of these anomalous positions are associated with the dimmest of the guide stars, with instrumental magnitudes of 5 or greater. Errors in onboard centroid determination due to competing background radiance are most likely responsible for this behavior.

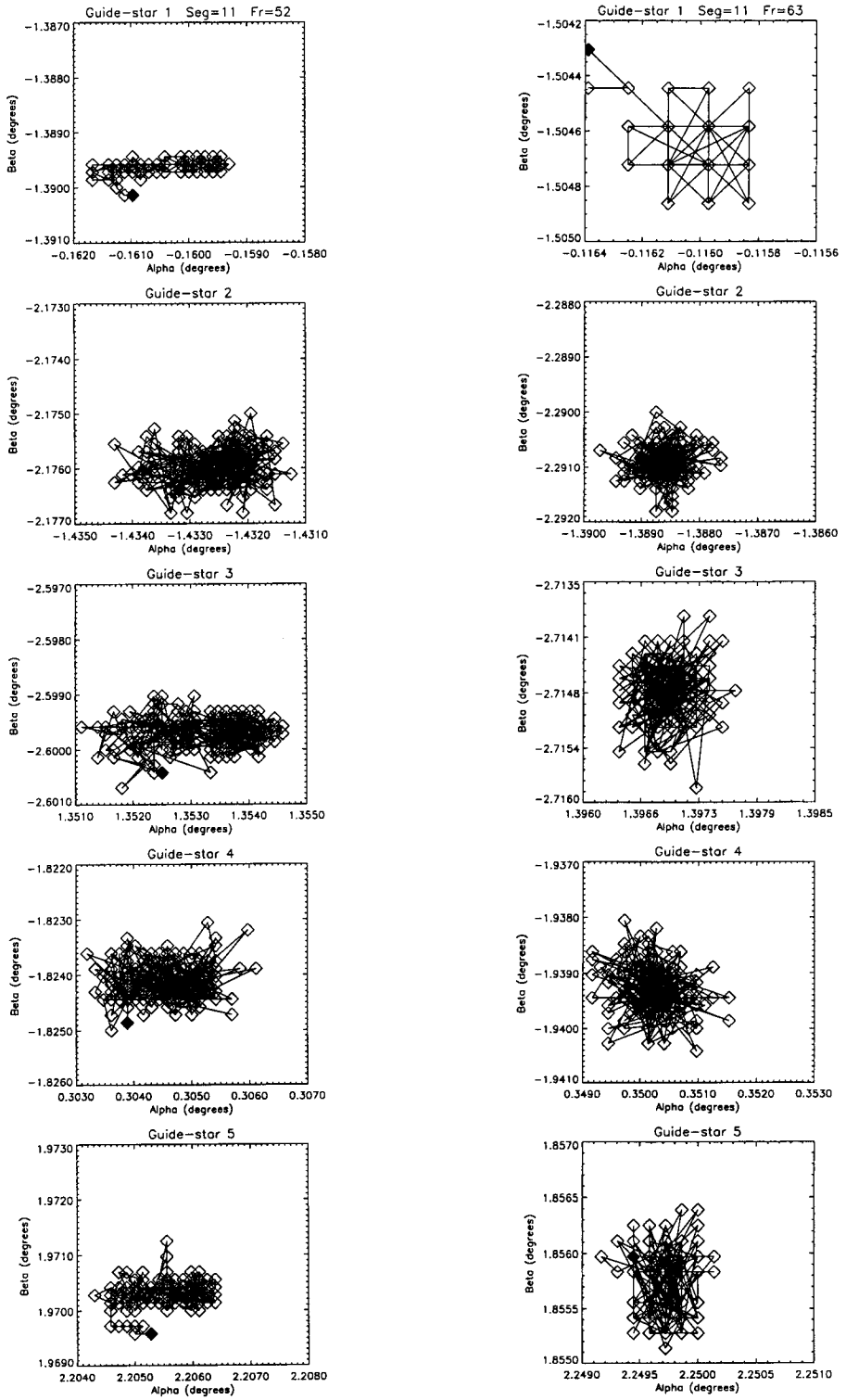

Figure 5.2-1. Guide-star positions versus time for the A) first and B) last frames of a typical observation segment.

Out of a total of 144 data frames for day 85, and 81 data frames for day 140, only two data frames (less than 1%), one from each day, showed very anomalous dispersions in the guide-star positions sampled over the frame-time period. In the case of the anomalous day-85 frame, the star-tracker was on target for the first ~40 seconds of the frame time, and then it inexplicably slewed off-target. In the case of the anomalous day-140 frame, the star-tracker apparently got confused, even though five guide stars were uploaded for this target, and one of the guide stars, Alpha Ursa Major, is fairly bright (with an instrumental magnitude of 1.5). In fact, this star was actually an asteroseismology target for this data frame, which puts it within a couple of arcseconds of the star-tracker's optical axis. Glint or other irradiation from space debris or satellites is a possible explanation for these anomalies.

The scatter in guide-star position is characterized in Figure 5.2-2, which shows that the radial RMS position deviation is a nonlinear function of guide-star brightness. Each point in the figure is the RMS value computed over guide-star positions taken over a frame's worth of data. The RMS values are smallest for the brightest stars, and tend to increase for dimmer stars. The square symbols on the plot indicate outliers corresponding to RMS values for frames occurring right after a slew. These outliers were not included in calculations of the sample-number-weighted mean and standard deviation versus guide-star magnitude, which are shown on the plot as solid and dotted lines.

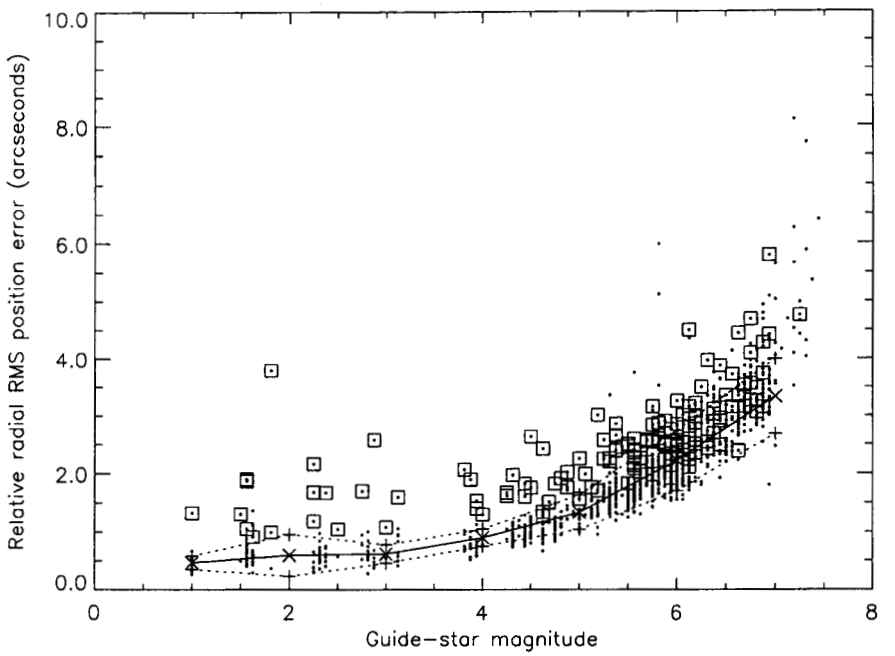

Figure 5.2-2. Radial RMS position deviation versus magnitude for guide stars measured by the WIRE star-tracker.

Table 5.2-1 gives the sample-number-weighted averages and standard deviations of the radial RMS position deviation as a function of guide-star magnitude. The average RMS value for the dimmest stars is a factor of more than 7 greater than for the brightest stars, with a standard deviation that is greater by more than a factor of 5 as well. The two largest RMS values occur for stars that are among the dimmest in the available data, and correspond to 35-second data frames containing only a couple of 10-Hz samples where the star tracker had actually locked onto the stars.

The guide-star positions presented as a function of guide-star brightness show increasing relative position error for progressively dimmer stars. These results characterize the performance of Ball's onboard r-centroiding algorithm for determining star positions from raw image data. The largest change in relative position error occurs for stars in the 6.5-7.5 magnitude range, which is the dimmest range for which data were available. Ball's recommended guide-star magnitude range is [1.0, 6.2].

Table 5.2-1. Average radial RMS position deviation versus magnitude for guide stars measured by the WIRE star-tracker.

Magnitude range	Number of RMS values*	Average (arcseconds)	Standard deviation (arcseconds)
0.5-1.5	10	0.47	0.12
1.5-2.5	64	0.59	0.36
2.5-3.5	31	0.62	0.16
3.5-4.5	75	0.90	0.15
4.5-5.5	177	1.34	0.29
5.5-6.5	424	2.22	0.52
6.5-7.5	180	3.34	0.66

*RMS values for up to 5 stars are available for each frame. These RMS values are averaged in separate magnitude bins to get the results in this table.

5.3 Attitude Errors

We define the attitude error as the difference between the commanded target quaternion and the mean of the actual attitude as determined from least-squares fits of the star-tracker measurements to the guide-star catalog positions. The means were computed by averaging the fit results for each individual frame. The sample-number-weighted averages of these means over all frames considered were also computed.

Figure 5.3-1 gives the distribution in frame number of the averages of the fit results for individual frames. Separate results are given for α and β dimensions, radial representation ($\sqrt{\alpha^2 + \beta^2}$), and roll angle. Evidence of residual slew motion is seen in the longer tail of the α-error histogram.

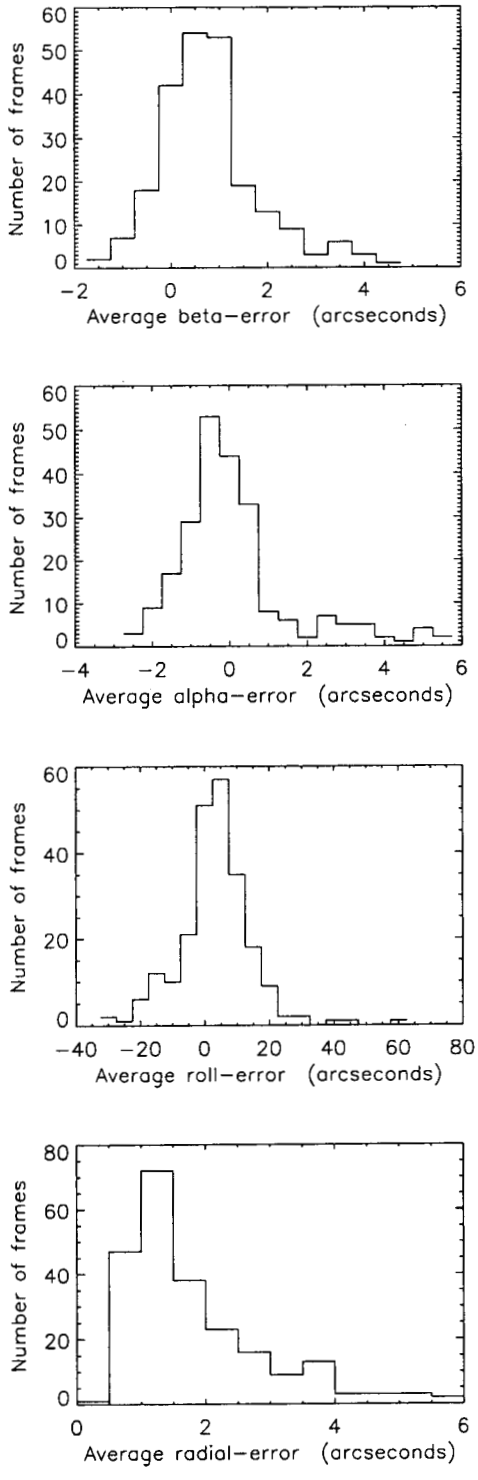

Figure 5.3-1. Frame-number histogram of the mean attitude errors.

Below in Table 5.3-1, we present overall statistical results for two different cases. The first case includes all frames in our two data sets, except for the two aforementioned anomalous frames (223 frames total). The second case is for a subset of these data that excludes either the first frame after each slew or the first 1000 samples (covering 100 seconds) of long frames containing many thousands of samples (202 frames total).

Table 5.3-1. Weighted means and standard deviations of the attitude errors. The standard deviation is given in parentheses.

Statistic	**Including all data frames* (arcseconds)**	**Excluding data frames following slew* (arcseconds)**
Mean α error	0.033 (1.31)	-0.34 (0.88)
Mean β error	0.71 (0.84)	0.75 (0.87)
Mean radial error	1.63 (0.90)	1.44 (0.70)
Mean roll-angle error	1.80 (11.7)	1.81 (11.2)

* Excluding the two aforementioned anomalous data frames.

The results show that, on average, the WIRE ACS/ST system is capable of pointing within about 1.7 arcseconds of the commanded target. The associated standard deviations are under an arcsecond. There is a significant change in the mean α error depending when after the slew it is computed; no such dependence is evident for the β and roll dimensions.

Considering only the <60-second data frames that occur right after each slew, the sample-number-weighted mean error in the α dimension, along which the slewing predominantly takes place, is about 3.6 arcseconds. This value is larger than the values given in Table 5.3-1 because the slew drift is still significant after the settle flag is set, and diminishes to about 1.44 arcseconds, on average, over about the next 100 seconds.

In order to reveal the underlying controlled motion of the spacecraft, we smoothed the curves of boresight pointing and roll versus time by averaging over a two-second sliding window. We found evidence in most of the curves that there are sinusoidal-like variations with periods ranging from 6-8 seconds, which is consistent with the bandwidth of the controller. These smoothed curves have characteristics that are very similar to those modeled for the WIRE ACS at GSFC. The autocorrelations of these smoothed curves show many peaks and valleys with correlation coefficients greater than 0.2 in absolute value; peaks this large are typically seen in the first 20 seconds of lag. It is also interesting to note that the resulting curves from subtracting the smoothed curves from their original curves appear to be uniformly distributed noise. The sum of variance of the noise and smoothed curves are very close to the variance of the original, which suggest that the two contributions are independent.

5.4 Attitude Stability

We characterize the attitude stability by the RMS deviations from the median boresight position of the frame, where the boresight positions have been determined from least-squares fits of the star-tracker measurements to the guide-star catalog positions. The RMS values were computed for each individual frame. Sample-number-weighted averages of these quantities were also computed over all frames considered.

Figure 5.4-1 gives the distribution in frame number of the RMS values of the fit results for individual frames. Separate results are given for α and β dimensions, radial representation ($\sqrt{\alpha^2 + \beta^2}$), and roll angle. Evidence of residual slew motion is clearly seen in the longer pronounced tail of the RMS α histogram.

The results presented in Table 5.4-1 are overall mean RMS values, computed by first finding the RMS value for each individual frame and then by computing sample-number-weighted averages of the RMS values over all frames of interest.

Table 5.4-1. Weighted means and standard deviations of RMS jitter. The standard deviation is given in parentheses.

Statistic	Including all data frames* (arcseconds)	Excluding data after slew* (arcseconds)
RMS α relative error	0.84 (0.42)	0.51 (0.18)
RMS β relative error	0.52 (0.17)	0.51 (0.17)
RMS radial relative error	1.02 (0.40)	0.73 (0.23)
RMS roll-angle relative error	11.3 (3.9)	11.1 (3.5)

* Excluding the two aforementioned anomalous data frames.

Overall, RMS radial jitter in the pointing is approximately one arcsecond, according to Table 5.4-1.

When data taken within the first 60 seconds after the slew is excluded, the pointing jitter decreases to about 0.7 arcseconds. The β and roll jitter are insensitive to when they are measured after the slew settle flag is set.

For comparison with the results in Table 5.4-1, the <60-second data frames that occur directly after a slew have a sample-number-weighted RMS radial jitter value of about 1.7 arcseconds.

The fine attitudes computed onboard the spacecraft are comparable to our least-squares-fit results, except that the former has a lower variance due to noise removal by the Kalman filter. The RMS deviations from the median are ~25% lower in pointing, and a factor of ~8 lower in roll.

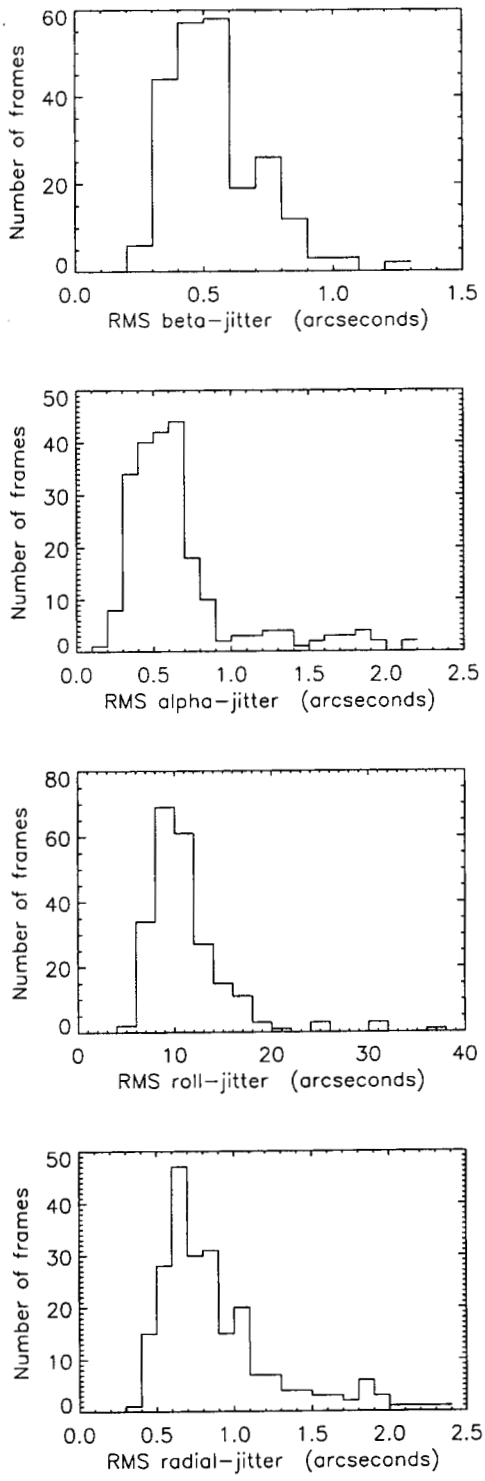

Figure 5.4-1. Frame-number histogram of the RMS attitude jitter.

5.5 Correlation with Guide-Star Parameters

We plotted attitude error and stability measures against four different parametrical characterizations of the guide-sets used by star tracker to acquire and hold its target, listed as follows:

1. Number of guide stars;
2. Maximum guide-star separation;
3. Minimum guide-star magnitude; and
4. Distance of brightest guide-star to the ST's FOV center.

Figure 5.5.1 presents the distributions of these guide-star parameters in the number of frames available in our day 85 and 140 data sets. The pointing error and stability versus the different guide-star parameters are shown in Figures 5.5-2 through 5.5-5. A solid circle represents each data frame. The solid curves (with × symbols) and the dotted curves (with + symbols) are the means and standard deviations computed as a function of the relevant guide-star parameter. The open square symbols denote the excluded data frames from these statistical calculations, which are the frames that directly followed the spacecraft's target-to-target slews, and therefore contain residual attitude drift.

The figures show that no strong trends in either pointing error or jitter are evident as a function of these guide-star parameters.

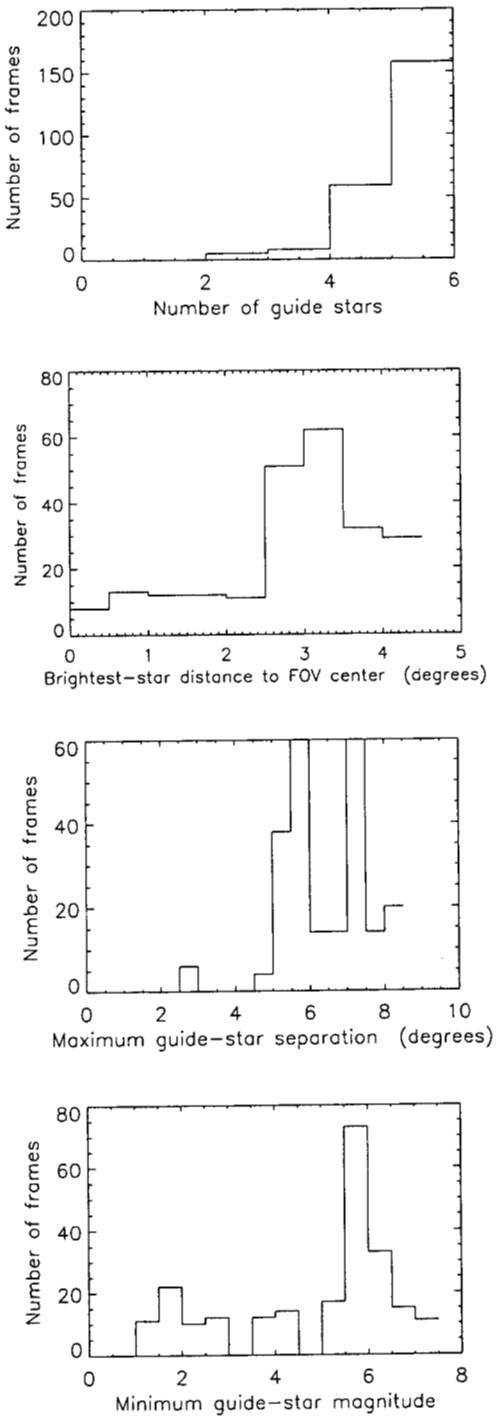

Figure 5.5-1. Histograms of the selected guide-star parameters versus number of frames in the data set studied.

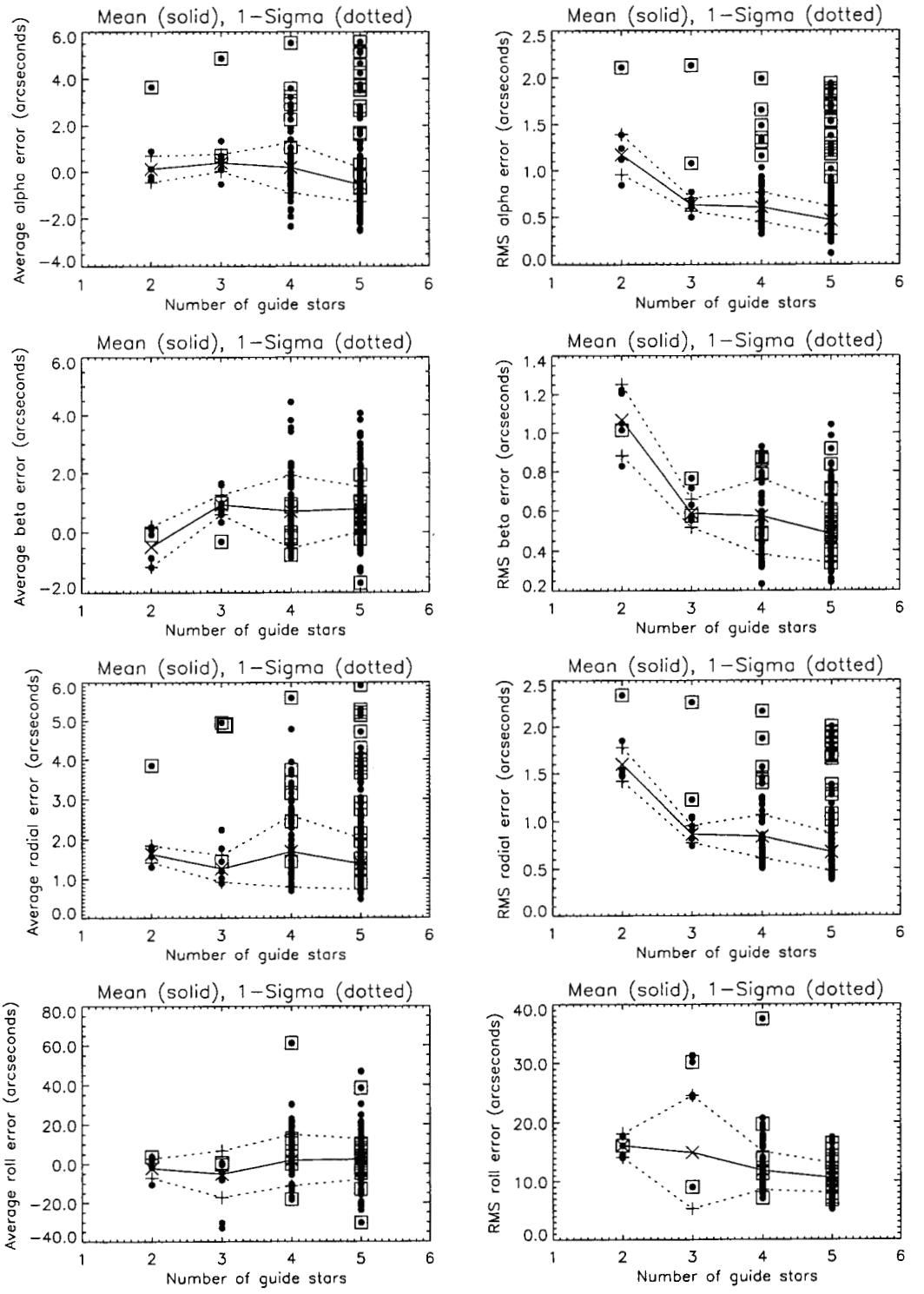

Figure 5.5-2. Attitude error and stability versus number of guide stars.

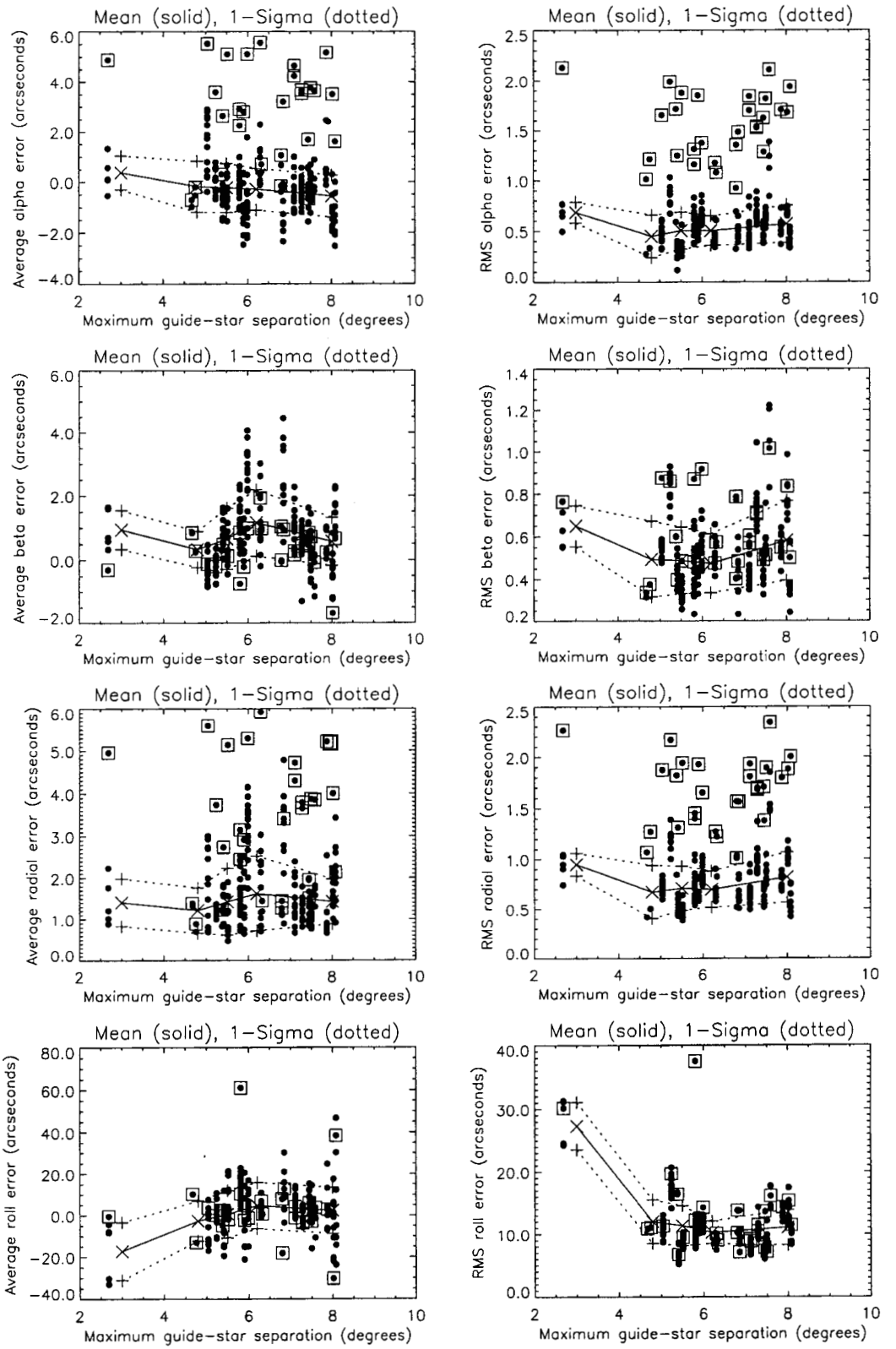

Figure 5.5-3. Attitude error and stability versus maximum guide-star separation.

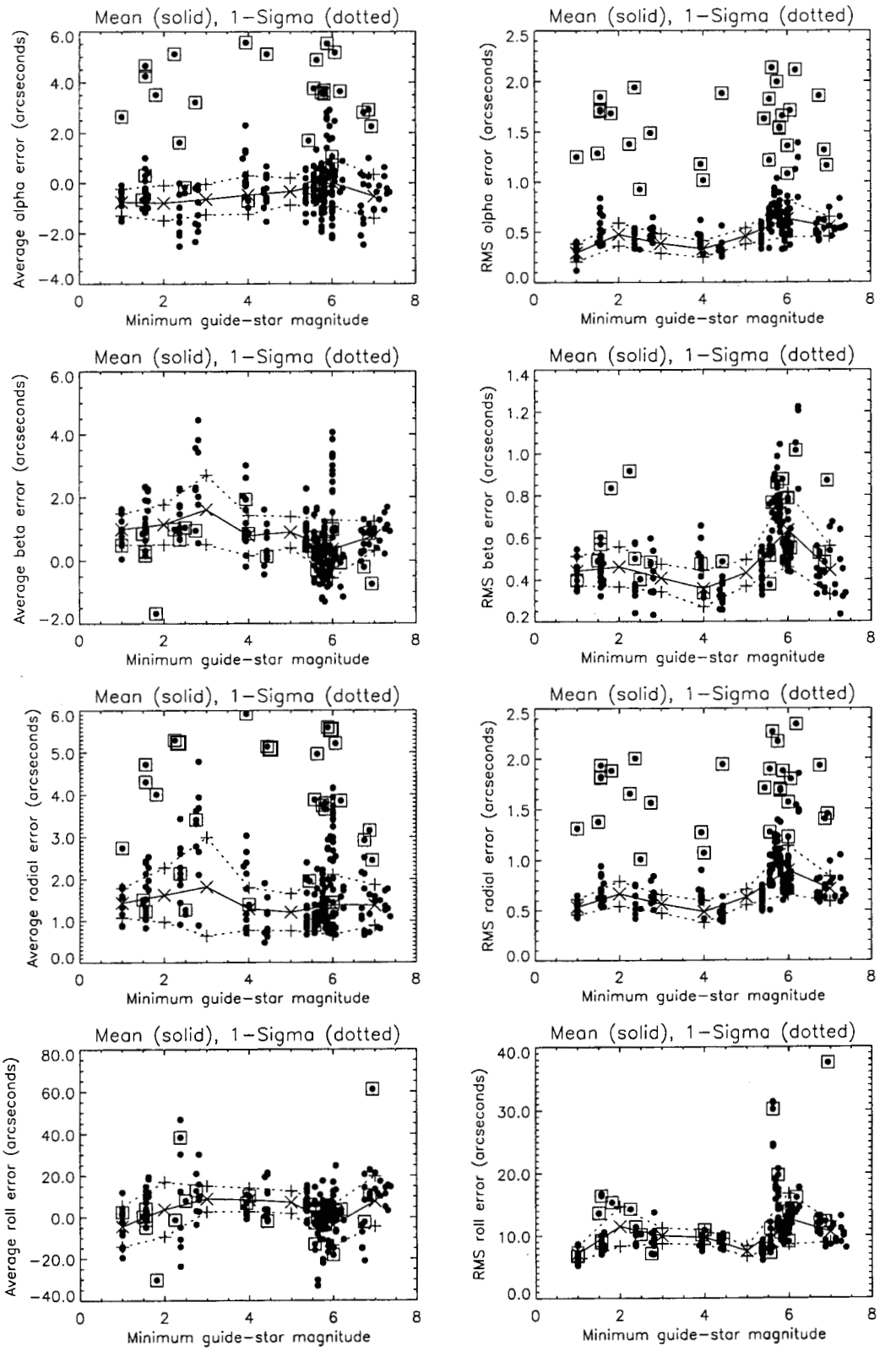

Figure 5.5-4. Attitude error and stability versus minimum guide-star magnitude.

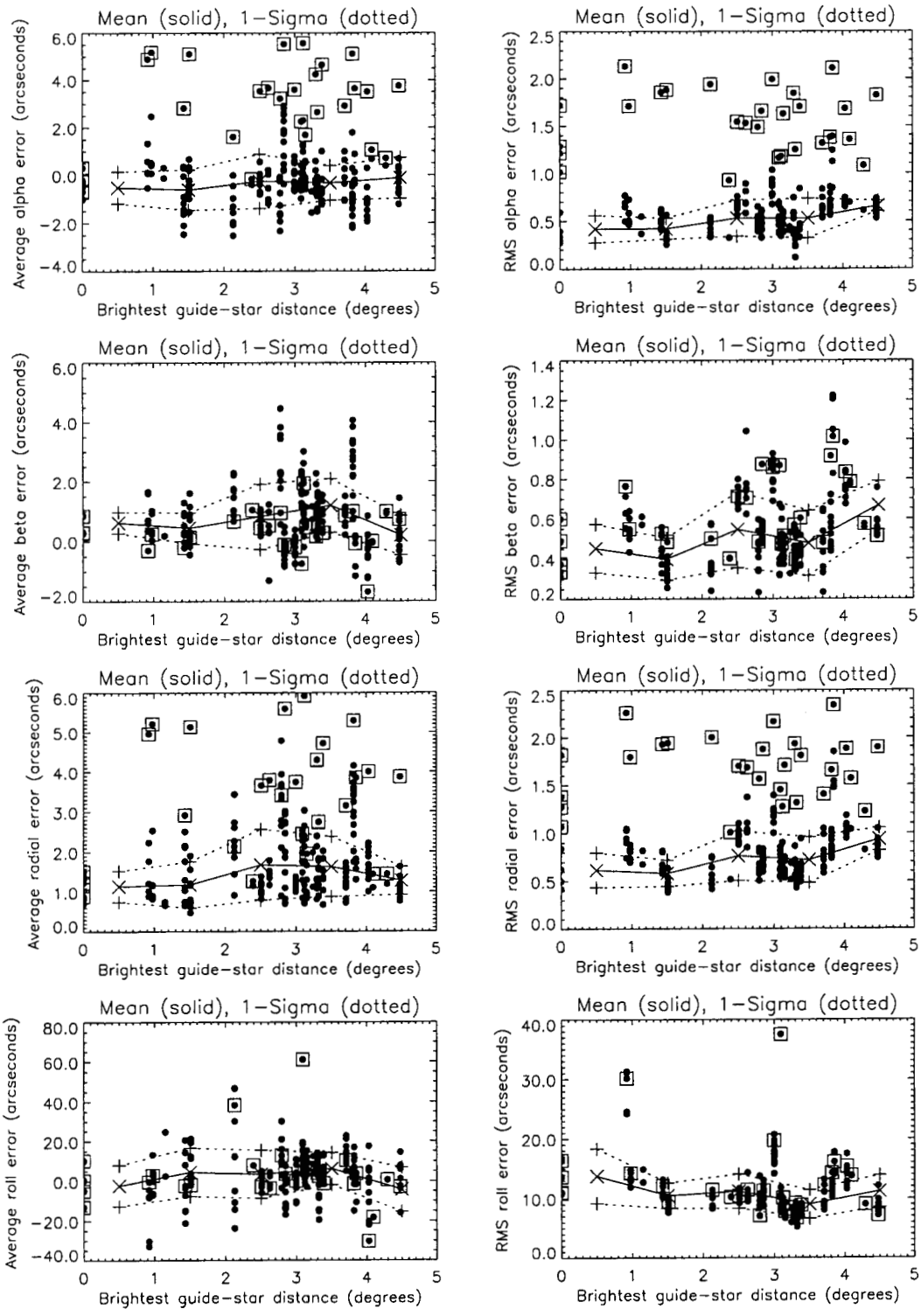

Figure 5.5-5. Attitude error and stability versus distance of brightest guide-star to the ST's FOV center.

5.6 Slew, Settle, and Dither Times

In this section, we present average slew, settle, and dither times. These characterize the times required to maneuver from target to target, and to make small dithers (<8 arcminutes) in the spacecraft pointing relative to a target. First, we give the working definitions of the slewing, settling and dithering states that we adopted for purposes of analyzing the ACS data. The definitions are based on values of several telemetry points, which determine the state of the ACS and are also sampled at 10 Hz.

5.6.1 Definitions

The beginning of the slewing state is defined by the transition of the ST to the standby state, together with the unsetting of the ACS settle flag. The end of the slewing state is defined by the transition of the ACS to the state where the fine-pointing gains are first used. According to the WIRE ACS Flight Software Users Guide, Section 2.2.2.3, this transition indicates that the spacecraft has maneuvered to within ~412 arcseconds of the estimated slew target. In plain language, the slewing state starts when the spacecraft maneuvers off its current target and ends when the spacecraft pointing, as determined by the gyro-based attitude solution, is sufficiently close to the next target.

The beginning of the settling state is defined by the transition of the ACS to the state where the fine-pointing gains are used. (The spacecraft uses a different set of gains to perform slewing and settling; the settling gains are normally maintained throughout the observation segment.) When the spacecraft closes to within ~360 arcseconds of its target, the ST begins acquiring the guide stars that are associated with the new target. The end of the settling state is defined by the setting of the ACS settle flag, together with the ST transition to the guide-star tracking state.

As delimited in Section 2.2.2.4 of the WIRE ACS Flight Software Users Guide, there are three requirements must be satisfied while the ACS is in the settled state.[7] The spacecraft must detect that it is pointing within 10 arcseconds of its target. The estimated body rotation rate must be less than 10 arcseconds per second. And the Good Star Condition must be met, which is that the pair-wise sum of the distances squared among the guide stars must be greater than 4 degrees squared.

The dithering state begins when ACS settle flag is unset, and the dither index changes while at the same time the ST remains in the guide-star tracking state. The dithering state ends when ACS settle flag is set while at the same time the ST remains in the guide-star tracking state.

Angles used as the abscissa in the plots given in the next section are values of the separation angle between the target and ST boresight position, which is given by the coarse attitude solution.

5.6.2 Results

Settle time is plotted versus slew angle in Figure 5.6.2-1. The data set consists of 29 slews, 15 from day 84 and 14 from day 140. Only a slight correlation of these two quantities is evident, and the scatter and distribution of the measurements from both days are consistent. The mean settle time is 6.64 +/- 0.14 seconds, with a sample standard deviation of 0.73 seconds.

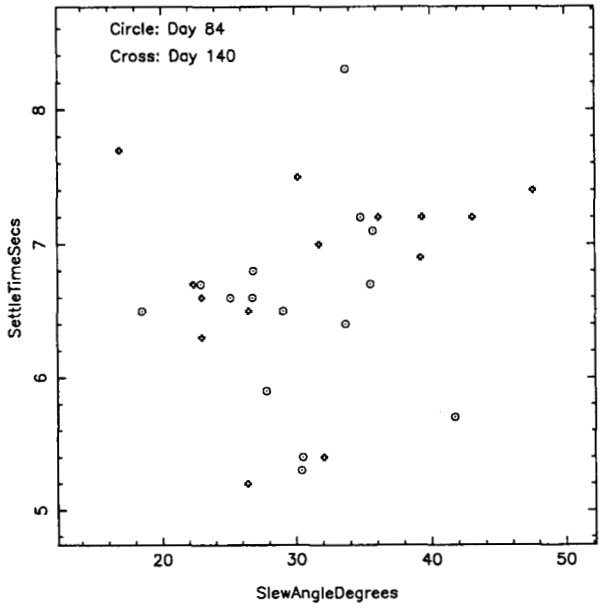

Figure 5.6.2-1. Settle time versus slew angle.

As a measure of how long one must wait between science observations with an intervening slew, the total slew time is equal to the sum of the slew and settle times. The total slew time versus slew angle is presented in Figure 5.6.2-2 using the 29 data points from both days. The linearity of the dependence of total slew time on slew angle is evident for slew angles in the range of approximately 15 to 50 degrees. Again, the range and spread in the data between both days are consistent.

The population for the dither time study comprised 192 dither maneuvers, of which 127 were from the day-84 data set and the remaining 65 were from the day-140 data set. Figure 5.6.2-3 shows dither time plotted against dither angle, and reveals that for dither angles between roughly 0.5 and 7 arcminutes, the dither time depends non-linearly on dither angle, and the dither times are between 4.5 and 5 seconds for the larger dithers.

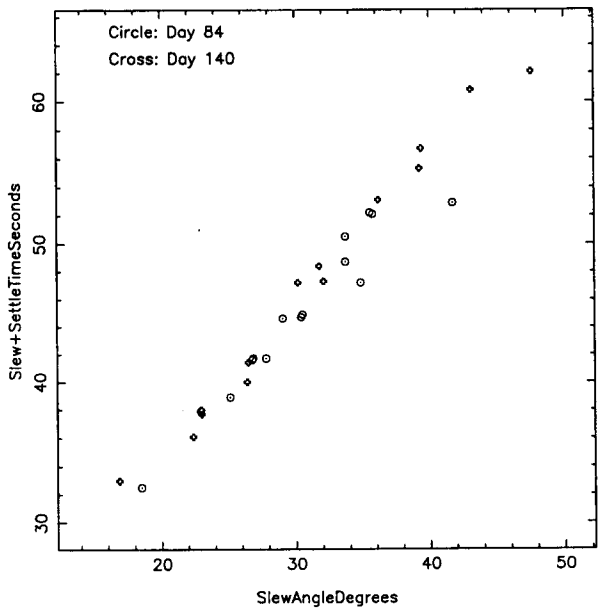

Figure 5.6.2-2. Settle-plus-slew time versus slew angle.

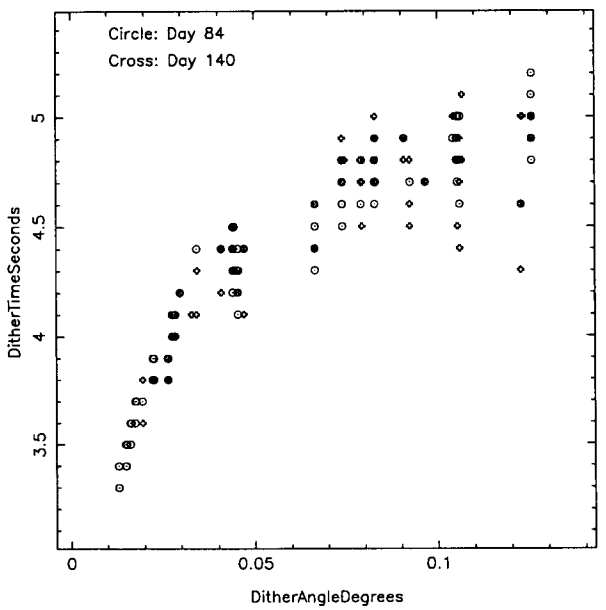

Figure 5.6.2-3. Dither time versus dither angle.

5.7 ZSP and SCS Safeholding

On-orbit tests have shown the WIRE spacecraft correctly transitions from stellar pointing to zenith sun pointing when Sun viewing-constraints are violated. This has been demonstrating numerous times when viewing several different targets. During one particular sequence of asteroseismology observations starting on July 8, 1999 at 0 GMT, Epsilon Ursa Majoris in the northern galactic hemisphere was observed, followed by Alpha Centauri in the southern galactic hemisphere. Upon completion of these targets the WIRE scheduler software inserted an "auto-filler" observation to have the spacecraft deliberately pointed somewhere while waiting for Epsilon Ursa Majoris to come back in view. For this particular auto-filler target the slew angle from Alpha Centauri is 111 degrees, which is longer than the usual case. During the slew, a Sun-viewing constraint was violated (a simplifying assumption in the WIRE scheduler software occasionally allows observations that will violate Sun viewing-constraints during a slew), and the spacecraft immediately transitioned to ZSP within 0.5 degrees of the violation point. Normal stellar-pointing operations resumed when the Epsilon-Ursa-Majoris observation segment initiated. This ZSP event occurred every orbit for several weeks, until a different sequence targets was scheduled.

On another occasion, when GSFC personnel were "parking" the WIRE spacecraft for the weekend, an inadvertent SCS-safeholding event occurred. During this normal operation, GSFC personnel would manually command the spacecraft to transition to ZSP on Saturday night just before end of the timelines buffered onboard. On Saturday, June 12, 1999, when this SCS safeholding occurred, the onboard Sun viewing-constraint table for stellar pointing had recently been modified with more relaxed values to facilitate asteroseismology observations. However, the separate onboard Sun viewing-constraint table for zenith sun pointing had not yet been modified, and so it still contained the original values for the primary mission. When the spacecraft was commanded to transition to ZSP from stellar pointing, where it happened to be violating primary mission constraints but not the relaxed constraints, an SCS-safeholding event correctly occurred. In retrospect, this event could have been predicted, had it been realized that the onboard stellar-pointing and ZSP constraint tables were different. Instead, it turned out to be a convenient, but unplanned, SCS-safeholding test. The transition occurred and the spacecraft properly executed the SCS-safehold control mode.

5.8 Moon Interference

The ability of the ST to operate near the Moon was tested by pointing at fixed celestial targets near the Moon and allowing the Moon to "walk" through the ST field of view on subsequent orbits. These tests show that the ST can be pointed close to the Moon and still function correctly, as long as the Moon does not fall within the ST's field of view. When the Moon does fall within the 8-degree x 8-degree field, the ST telemetry flag indicating a saturated background is activated. No stars can be tracked, and the ACS falls back to TSA mode after an approximately two-minute timeout expires. The fact that the

system works with the Moon just outside the ST field validates the straylight design of the tracker.

6.0 Discussion and Conclusions

Our analysis results clearly show that the WIRE attitude control system, star tracker, many housekeeping data acquisition and handling systems, and communications hardware systems worked admirably, and well within their design requirements. This includes up through and many months beyond its four-month nominal mission lifetime.

No appreciable differences are evident between the statistical properties of the day 85 and day 140 data sets, which were acquired almost two months apart. These two data sets are representative snapshots of the spacecraft's performance after one and three months, respectively, of the four-month nominal mission. Although a similar analysis has not been carried out for ACS and star-tracker data acquired later, the WIRE spacecraft was used almost daily for asteroseismology observations, starting from mid-March to when this paper was submitted for review (11/11/99). Asteroseismology observations are tentatively scheduled to continue into the year 2000.

The measured mean pointing accuracy of 1.6 arcseconds with a standard deviation of 0.9 arcseconds is well within the 1-arcminute requirement, and better than the 2-arcsecond goal. The measured mean roll accuracy of 1.8 arcseconds with a standard deviation of 11.7 arcseconds is also well below the 9.5-arcminute roll-angle re-pointing requirement. The approximately one-arcsecond RMS radial jitter derived from star-tracker data is much less than the 6-arcsecond requirement for the telescope. Thus there is plenty of margin for additional possible jitter caused by mechanical vibrations of the telescope relative to the star tracker, which, moreover, are expected to be relatively small because of WIRE's graphite composite structure.

The residual drift was expected, and also showed up in pre-launch simulations. The settle flag is set when the drift decreases to a tolerable level, which was a trade-off between data-collection time and image resolution for the first few images directly following the slew. Our results show that an additional 10-30% decrease in the measured pointing error and jitter can be realized by discarding the first 100 seconds worth of data after the settle flag has been set. However, this would not be warranted for the WIRE mission because these improvements are small relative to point-spread function widths of primary science instrument, which ranged from 21-25 arcseconds with a relatively small amount of widening caused by spacecraft jitter. For other missions with more stringent requirements, this information may be useful.

7.0 Acknowledgements

We gratefully acknowledge the support of WIRE personnel at NASA headquarters for this work, and the entire WIRE team at NASA Goddard Space Flight Center, Caltech's

Infrared Processing and Center, and USU's Space Dynamics Laboratory for helping to implement the project. Special thanks to David Henderson for scheduler support, Mike Prior and his excellent team for efficient mission operations support, and Mike Paoletta, Maxine Russell, and Marylin Glass for timeline processing and uplink support. The WIRE project is the result of hard work by many other NASA professionals too numerous to mention here -- Thank you all for your dedication and hard work.

Chuck Clagett was selected as NASA Inventor of the Year in March 1999 for his design of SMEX reactions wheels, which are used on the WIRE spacecraft.

8.0 References

1. Fennell, M. D., V. Z. Untalan III, and M. H. Lee, "The Attitude Control System Design For The Wide-Field Infrared Explorer Mission," Proceedings of the 11th Annual AIAA/USU Conference on Small Satellites, Logan, Utah, September 1997.

2. Buzasi, D., J. Catanzarite, R. Laher, T. Conrow, T. Kreidl, T. Gautier, David Shupe and others TBD, "The Detection of Multimodal Oscillations on α UMa," Submitted to Astrophysical Journal Letters, 1999.

3. Hacking, P., T. N. Gautier, T. L. Herter, C. J. Lonsdale, D. L. Shupe, G. Stacey, H. R. Schember, B. T. Soifer, M. W. Werner, P. Graf, S. H. Moseley, and J. R. Houck, "The Wide-Field Infrared Explorer (WIRE) Mission," Proceedings of the Moriond Astrophysics Meeting on Extragalactic Astronomy in the Infrared, Moriond, France, March 1997.

4. Stoneking, E. T., "A Robust Star Acquisition Algorithm for the Wide-Field Infrared Explorer", AAS 98-367, Proceedings of the AAS/GSFC International Symposium on Space Flight Dynamics, NASA Goddard Space Flight Center, Greenbelt, Maryland.

5. Hacking, P., H. Schember, T. Herter, T. N. Gautier, B. Fafaul, H. Ames, D. Everett, J. Kemp, T. Conrow, and D. Henderson, WIRE Science and Instrument Functional Requirements, Version 1.4, JPL D-13132, January 22, 1997.

6. Private communication between Russ Laher and Dick Deters of Ball Aerospace, June 3, 1999.

7. Barnes, K. C., C. M. Melhorn, and T. Phillips, "The Software Design for the Wide-Field Infrared Explorer Attitude Control System," Paper No. SSC98-VIII-2, AIAA Conference on Small Satellites, Logan, Utah, September 1998.